

Understanding the Curious Magnetic State of Sr_3OsO_6

Shreya Das,¹ Anita Halder,¹ Atasi Chakraborty,² Indra Dasgupta,² and Tanusri Saha-Dasgupta^{1,*}

¹*Department of Condensed Matter Physics and Material Sciences,
S. N. Bose National Centre for Basic Sciences, JD Block,
Sector III, Salt Lake, Kolkata, West Bengal 700106, India.*

²*School of Physical Science, Indian Association for the Cultivation of Science, 2A & 2B,
Raja Subodh Chandra Mallick Rd, Jadavpur, Kolkata, West Bengal 700032, India.*

Motivated by the recent report on high T_c ferromagnetic insulating state of single transition metal containing double perovskite compound, Sr_3OsO_6 (Wakabayashi et. al., Nature Commun **10** 535, 2019), we study this curious behavior by employing first-principles calculations in conjunction with exact diagonalization of full t_{2g} multiplet problem of two Os sites. Our analysis highlights the fact that stabilization of Sr_3OsO_6 in the cubic phase in epitaxially grown thin film is the key to both ferromagnetic correlation and high temperature scale associated to it. This also provides a natural explanation for the sister compound, Ca_3OsO_6 to exhibit low T_N antiferromagnetism in its monoclinic structure. Further the insulating property is found to be driven by opening of Mott gap in the half filled spin-orbit coupled $j = 3/2$ manifold of d^2 Os. We point out that $\text{Sr}_2\text{CaOsO}_6$ which naturally forms in the cubic phase would be worthwhile to explore as a future candidate to exhibit high T_c ferromagnetic insulating state in bulk form.

PACS numbers:

INTRODUCTION

Ordered double perovskite compounds derived out of ABO_3 perovskites (A = alkaline earth/rare earth, B = transition metal) with half of the B sites substituted by B' , and rock-salt ordering of B- B' , extending the formula to $\text{A}_2\text{BB}'\text{O}_6$ have attracted significant attention primarily due to their intriguing electronic and magnetic properties.[1–3] This includes above room temperature half metallic behaviour in compounds like $\text{Sr}_2\text{FeMoO}_6$ with transition temperature (T_c) of 420 K,[6, 7] $\text{Sr}_2\text{CrMoO}_6$ ($T_c = 420$ K),[8, 9] Sr_2CrWO_6 ($T_c = 458$ K),[10, 11] $\text{Sr}_2\text{CrReO}_6$ ($T_c = 620$ K),[12] ferromagnetism in $\text{Ca}_2\text{MnOsO}_6$,[4] and Dirac-Mott insulating state in $\text{Ba}_2\text{NiOsO}_6$,[5] While all the above examples include two transition metals (TMs) at B and B' sites, double perovskites with a single transition metal have been also synthesized. Most of these single TM containing double perovskites like $\text{Ba}_2\text{CaOsO}_6$,[13] $\text{Sr}_2\text{MgOsO}_6$,[14, 15] $\text{Ca}_2\text{MgOsO}_6$ [14] or Sr_2YReO_6 [16] are either antiferromagnets or exhibit spin glass like behavior. The report of Sr_3OsO_6 [18] double perovskite, containing a single $5d$ TM in B- B' sublattice, exhibiting ferromagnetic (FM) insulating state at a temperature ≈ 1060 K is thus unexpected and counter-intuitive. It is surprising on several counts. Firstly the TM-TM magnetic interaction is expected to be hindered by the presence of a non magnetic Sr ion at B' site in the B-O- B' -O-B super-exchange path. Secondly the high T_c is expected to be a property of $3d$ TM containing compounds, rather than $5d$ TM containing compounds. Thirdly, most known ferromagnets are metals while insulating properties are attributed to antiferromagnets. Few known examples of ferromagnetic insulators are low T_c materials e.g. EuO (77 K),[19] CdCr_2S_4 (90 K),[20] SeCuO_3 (25 K)[21] with the exception of $\text{La}_2\text{NiMnO}_6$,[22] another FM insulating double perovskite with a T_c of 280 K, which is still about a factor of 3-4 smaller compared to that reported for

Sr_3OsO_6 .

The situation becomes further puzzling by the fact that replacement of Sr by Ca makes the compound antiferromagnetic (AFM) with low transition temperature (≈ 50 K).[23] It is curious to note while the crystal structure of the reported[18] high T_c ferromagnetic insulating compound Sr_3OsO_6 is cubic, that of Ca_3OsO_6 is monoclinic, prompting the role of crystal structure in influencing the magnetic behavior of these compounds. Os being a $5d$ element, the role of spin-orbit coupling (λ) becomes important and adds another dimension to the problem in addition to onsite Coulomb repulsion U and Hund's coupling parameter J_H within the multi orbital framework of Os t_{2g} 's. Understandably the interplay of crystal geometry, spin orbit coupling, Coulomb repulsion and Hund's coupling governs the exotic state of Sr_3OsO_6 .

In the following we unravel this interplay by employing first-principles density functional theory calculations, constructing low energy model Hamiltonian in first-principles derived Wannier basis and performing exact diagonalization calculation of a two Os site full multiplet problem with realistic parameters. Our analysis reveals that ferromagnetism in cubic symmetry gets stabilized for a large range of U and J_H , assisted by appreciably large nearest neighbor Os-Os hopping across the face of the cube of the double perovskite structure. Suppression of this hopping in distorted monoclinic symmetry destabilizes ferromagnetism and instead stabilizes antiferromagnetism. The stabilized ferromagnetic state in cubic symmetry gives rise to an insulating solution through formation of a spin-orbit coupled Mott state of d^2 , $j = 3/2$ Os t_{2g} 's. The reported[18] cubic symmetry of Sr_3OsO_6 , crucial for stabilization of ferromagnetic state, turns out to be not the natural choice, rather formed in epitaxially grown thin film geometry. We propose $\text{Sr}_2\text{CaOsO}_6$ [24] to be an alternative natural candidate which should exhibit high T_c FM insulating state even in the bulk form.

COMPUTATIONAL DETAILS

The first-principles density functional theory (DFT) calculations are carried out for realistic description of the problem. For the purpose of calculation, two different basis sets, namely the plane wave basis[25] and muffin-tin orbital basis[26] are used. The agreement between the two sets of calculations are verified in terms of calculated density of states and band structures.

The structural optimization as well as the influence of spin-orbit coupling (SOC) and onsite correlation U on the electronic structure are investigated using plane-wave pseudopotential method implemented within the Vienna Ab initio simulation package (VASP).[27] In the plane-wave calculations the wave functions in the plane-wave basis are expanded with a kinetic-energy cutoff of 650 eV. For self-consistent calculations with plane wave basis the k-point meshes are chosen to be $6 \times 6 \times 6$ for the cubic structure, $6 \times 6 \times 6$ for the triclinic structure, and $6 \times 6 \times 4$ for the monoclinic structure. The convergence of the results in terms of choices of k-point mesh is checked by repeating calculations with $12 \times 12 \times 12$ (cubic), $12 \times 12 \times 12$ (triclinic) and $12 \times 12 \times 8$ (monoclinic) k-points. The calculations with larger k-points are found to effect the results only marginally, with maximum change in magnetic moment by $0.001 \mu_B$ and energy difference by 0.75 meV. Calculations are carried out with chosen exchange-correlation functional of generalized gradient approximation (GGA)[28] within the framework of Perdew-Burke-Ernzerhof (PBE).[29] The effect of SOC is included within GGA+SOC implementation of VASP. The effect of missing correlation effect beyond GGA at Os site is considered within GGA+SOC+ U framework[30] by varying the screened Hubbard U value within 2-4 eV and fixing the Hunds coupling J_H at 0.6 eV, with choice of fully localized limit (FLL) of double-counting, as implemented in VASP. The importance of Hubbard U parameter in description of properties of insulating $5d$ transition metal oxides have been stressed in a number of literature, especially in context of iridates for which description of its insulating behavior relies on formation of Mott insulating state within the spin-orbit coupled $j = 1/2$ manifold.[31] Estimated value of Hubbard U in Os oxides and compounds vary from about 2 eV[32, 33] to about 3.5 eV.[34] We thus choose U value to vary within the range 2-4 eV. Optimization calculations are done until all the forces on the atoms become smaller than 10^{-5} eV/Å.

The N-th order muffin-tin orbital (MTO) method, [35] which relies on self-consistent potential generated by the linear MTO (LMTO) [36] method, is used for constructing effective Os t_{2g} Wannier functions. The low-energy tight-binding Hamiltonian, defined in the effective Os Wannier basis provides the information of crystal-field splitting at Os site as well as effective hopping interactions between the Os sites. The latter is used as an input to exact diagonalization calculation of the two-site Os problem. The muffin-tin radii of the different atomic sites used in LMTO calculations are

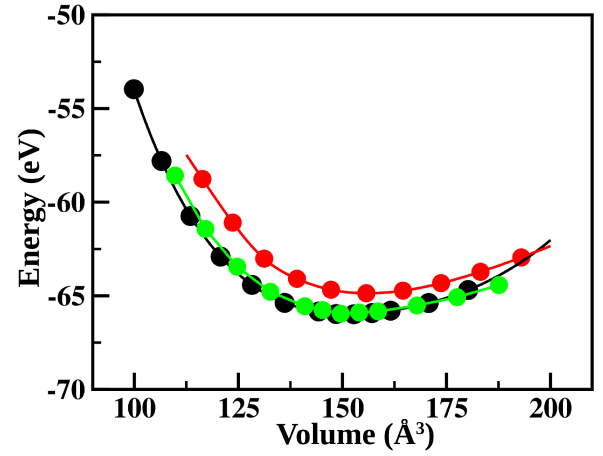


FIG. 1: (Color online) Comparison of total energy versus volume calculated within GGA+SOC+ U for Sr_3OsO_6 in cubic (red/dark grey), monoclinic (black) and triclinic (green/light grey) structures.

chosen as following, 2.36 Å (2.05/1.90 Å) for Sr_A , 1.71 Å (1.99/1.80 Å) for Sr_B , 1.25 Å (1.44/1.39 Å) for Os, and 0.87 Å (0.81/0.93 Å, 0.90/0.93 Å, 0.84/0.93 Å) for O atoms in the cubic (monoclinic/triclinic) structure of Sr_3OsO_6 .

RESULTS

Crystal Structure of Sr_3OsO_6

The ideal space group of rock salt ordered double perovskite is cubic Fm-3m, which is the crystal structure reported[18] for the Sr_3OsO_6 exhibiting high T_c ferromagnetic behavior. Tilting and rotation of BO_6 and $\text{B}'\text{O}_6$ octahedra leads to different lower symmetry non-cubic structures, tilt and rotation being governed by the tolerance factor, defined as $t_R = \frac{r_A + r_O}{\sqrt{2}(\frac{r_B + r_{B'}}{2} + r_O)}$ where r_A , r_B , $r_{B'}$ and

r_O denote the ionic radii of A site cation, B, B' cations, and O anion, respectively. Several different non-cubic structures have been reported for double perovskites, rhombohedral R-3, tetragonal I4/m and tetragonal I4/mmm, monoclinic $\text{P}2_1/\text{n}$, monoclinic C2/m, with rare examples of tetragonal $\text{P}4/\text{mn}$ and triclinic P-1.[2] Compounds with relatively smaller tolerance values, about 0.92 or less, are predominantly of monoclinic symmetry, while compounds with relatively larger tolerance factors, beyond 0.92 tend to form in either cubic, or tetragonal or rhombohedral symmetry. Considering the ionic radii of Sr^{2+} , Os^{6+} and O^{2-} , the tolerance factor of Sr_3OsO_6 turns out to be 0.89, similar to that of Ca_3OsO_6 . Therefore, there is high possibility that Sr_3OsO_6 grown under solid state reaction would form in non-cubic structure. In order to resolve this issue, we resort to genetic algorithm as implemented in USPEX (Universal Structure Predictor: Evolutionary Xtallography)[37] which has been demonstrated to predict accurate crystal structure of different multinary compounds,

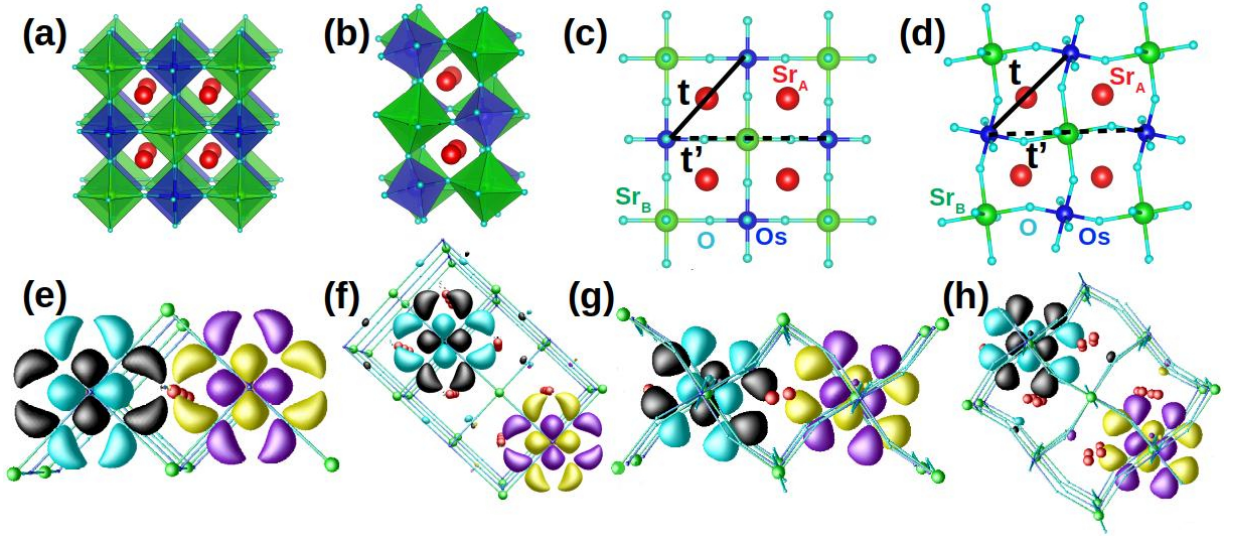


FIG. 2: (Color online) (a)-(b) The cubic and distorted monoclinic structures of Sr_3OsO_6 . The Sr atoms at A-sites (Sr_A) are marked as red (dark grey) balls, the Sr_BO_6 and OsO_6 octahedra at B and B' sites are marked in blue (dark grey) and green (light grey), respectively. (c)-(d) The nearest neighbor (t) and next-nearest neighbor (t') Os-Os hopping paths across the face and edge of the cube and distorted cube in cubic and monoclinic structures. (e)-(f) The overlap of Os effective t_{2g} Wannier functions placed at nearest neighbor and next nearest neighbor Os sites. Oppositely signed lobes of the Wannier functions are colored differently (cyan (light grey)/black for site 1 and magenta (dark grey)/yellow (white) for site 2). (g)-(h) Same as in (e)-(f) but shown for monoclinic structure.

including double perovskites.[38, 39] We apply the genetic algorithm based on our first-principles computed energies as goodness parameter, and comparing energies among a large number of competitive structures over a number of generations. Different structures in each generation are produced following different variational operations like heredity, mutation, permutation and those generated randomly. Application of genetic algorithm on Sr_3OsO_6 results in monoclinic $P2_1/n$ and triclinic $P-1$ as probable structures for Sr_3OsO_6 . We note that recent high pressure synthesis of Sr_3OsO_6 in powder form[40] did suggest monoclinic and triclinic structures as probable structures for Sr_3OsO_6 .

In order to rigorously check this issue, we carry out total energy versus volume calculation within GGA+SOC+ U scheme considering the genetic algorithm screened structures, *i.e.* monoclinic $P2_1/n$ and triclinic $P-1$, and the reported[18] cubic structure of Sr_3OsO_6 thin film. The results are presented in Fig. 1. Fig. 1 reveals that the energetics of monoclinic and triclinic phases are close with the energy of monoclinic phase at equilibrium volume being about 30 meV/f.u. lower than that corresponding to triclinic phase. The cubic structure of Sr_3OsO_6 reported in its thin film form[18] is, however, found to be off by a large energy difference of about 1.1 eV/f.u. from the lowest energy monoclinic structure. The crossover between lowest energy monoclinic and cubic symmetry would require a large tensile strain of about 6.5% which appears impractical to achieve. This is contrary to that reported in Ref. 18. This prompts us to conclude that the reported stabilization of Sr_3OsO_6 in cubic phase is presumably caused by the epitaxial growth of Sr_3OsO_6 in a molecular beam epitaxy set

up.

In the following we explore the magnetic properties of Sr_3OsO_6 considering the lowest energy monoclinic structure and the reported cubic structure in Ref. 18, in order to unravel the role of crystal structure.

NMTO-downfolding and Super-exchange paths

The 6+ nominal valence of Os ion in Sr_3OsO_6 results in d^2 occupancy. The octahedral crystal field of the surrounding oxygen environment splits the Os 5d levels into three t_{2g} 's and two e_g 's. Out of three t_{2g} levels thus two of the levels become half-filled, third one being empty. The empty e_g levels remain separated from t_{2g} 's by large energy splitting of ≈ 3 -4 eV, suppressing hopping processes involving e_g 's.

This in turn drives antiferromagnetic super-exchange coupling due to virtual hopping between half-filled t_{2g} orbitals at neighboring Os sites, and ferromagnetic super-exchange coupling due to virtual hopping between half-filled and empty t_{2g} orbitals at two Os sites. The resultant exchange is decided by the competition between the antiferromagnetic and ferromagnetic exchanges. For quantitative estimates of the relative strengths of these two competing interactions, a low energy Os t_{2g} Hamiltonian needs to be constructed. In order to have a realistic description of this Hamiltonian which incorporates the structural and chemical information correctly, we employ the NMTO-downfolding.[35] Following this procedure, the low energy tight-binding Hamiltonian is defined in effective Os t_{2g} Wannier basis, obtained by downfolding

or integrating out all the degrees of freedom including Sr, Os e_g , O p other than Os t_{2g} degrees of freedom. This results in Os t_{2g} effective Wannier functions with their head part shaped according to t_{2g} symmetry and tail part shaped according to integrated out orbitals. With a goal to uncover the influence of underlying crystal symmetry of Sr_3OsO_6 on magnetic properties, we construct the low energy Os t_{2g} Hamiltonian in effective Os t_{2g} Wannier basis for cubic symmetry of Fm-3m, as reported in Ref.18 and theoretically predicted lowest energy monoclinic $P2_1/n$ symmetry. The cubic and monoclinic structures are shown in panels (a) and (b) of Fig. 2 which features corner shared network of OsO_6 and Sr_BO_6 octahedra with Sr_A atoms occupying the void created by neighbouring OsO_6 and SrO_6 octahedra. Compared to ideal cubic structure, in monoclinic $P2_1/n$ structure the BO_6 and $\text{B}'\text{O}_6$ octahedra exhibit out of plane tilt and in-plane rotation. The face-centered cubic (FCC) lattice formed by Os ions in cubic structure thus distorts in the monoclinic structure with Os-O-Os angle across the face of the cube deviating from 90° and Os-O-Sr angle along the edge of the cube deviating from 180° . The deviations of these two angles in monoclinic phase are found to be $2\text{-}5^\circ$, and $30\text{-}40^\circ$ respectively.

Within the above structural framework, two possible Os-Os hopping paths are, a) the nearest-neighbour path (t) across the face of cube/distorted cube and b) the next nearest neighbour path (t') across the edge of the cube/distorted cube as shown in Figs 1(c) and (d) for the cubic/monoclinic structures. Following the conventional wisdom, the t hopping that proceeds through 90° or near 90° Os-O-Os is expected to be either zero or very weak. The hopping t' proceeding through linear or near linear exchange path of Os-O-Sr_B-O-Os mediated through non magnetic Sr is also expected to be weak. This makes high T_c ferromagnetism of Sr_3OsO_6 a puzzle.

Surprisingly, the overlap plots of NMTO-downfolding derived Os t_{2g} effective Wannier functions placed at nearest-neighbour Os sites reveal a remarkable trend. As is evident from Fig. 2(e), in the ideal cubic structure, the O p like tails of the Os t_{2g} Wannier functions strongly bend towards the Sr_A atom at A-site position, forming a well defined connected path between two Os sites across the face of the cube, mediating the t hopping. Moving to the monoclinic structure, the Wannier functions get misaligned due to the structural deviation from 90° (cf Fig. 2(g)), weakening the connected path between Os sites across the face. Due to this bending of the O- p like tail, on the other hand, the Wannier functions have hardly any overlap between two Os sites connected by t' hopping, separated by O-Sr_B-O across the edge (cf Figs. 2(f) and 2(h)).

The trend observed in Wannier function overlap plots gets reflected in the 3×3 tight-binding Hamiltonian constructed in Os t_{2g} NMTO-downfolding Wannier basis. The monoclinic distortion results in non-cubic crystal field splitting, lifting the degeneracy of t_{2g} levels, the non-cubic crystal field splitting being in the range of $0.07\text{-}0.10$ eV. The nearest neighbour hopping interaction, t which is a 3×3 matrix, following the expectation from Wannier function overlap plots, is found to be

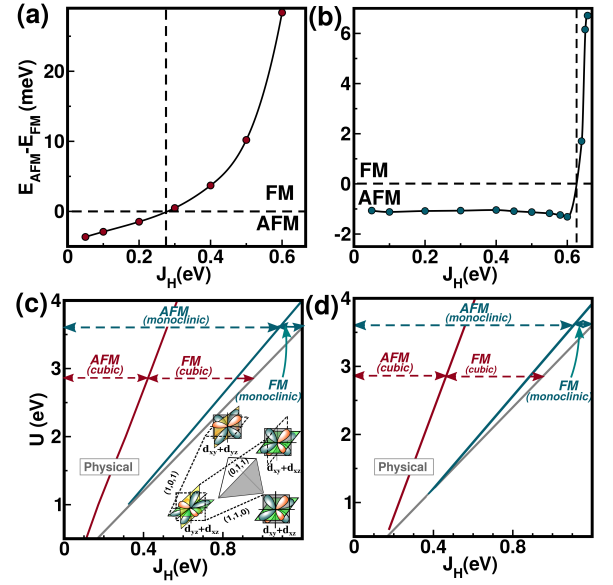


FIG. 3: (Color online) The energy difference between ferro and antiferro alignment with Os spins as a function of varying values of Hund's coupling, J_H , as given in exact diagonalization solution of a two-site Os t_{2g} full multiplet problem, fixing U at 2 eV and λ at 0.1 eV and considering the DFT derived hopping interaction in cubic symmetry (panel (a)) and in monoclinic symmetry (panel (b)) of Sr_3OsO_6 . (c) The U - J_H phase diagram showing the stabilization of ferro and antiferro alignment of Os spins in cubic and monoclinic phase, for choice of $\lambda = 0.2$ eV. The inset shows the ordering of Os t_{2g} orbitals, with occupancy of two of the Os $6+ d$ electrons reversing between d_{xy}/d_{xz} , d_{yz}/d_{xz} , d_{xy}/d_{yz} and d_{xy}/d_{xz} along the connecting vectors of Os FCC tetrahedra. (d) U - J_H phase diagram for choice of $\lambda = 0.4$ eV. The grey solid line in (c) and (d) demarcates the physically relevant space, $U' = U - 2J_H > J_H$.

significant with largest strength of 0.17 eV for cubic Sr_3OsO_6 . In the monoclinic phase, this hopping gets largely suppressed with largest strength of 0.05 eV. Compared to t , t' which is also a 3×3 matrix is found to be significantly smaller, the largest strength of t' being about 0.01 eV for the cubic phase, an order of magnitude smaller compared to that of t . For the monoclinic structure, this is found to be negligibly small. In the exact diagonalization calculations, presented in the following section, only the effect of hopping t is thus considered, ignoring the small hopping, t' .

Two-site Model and Magnetic Phase Diagram

Armed with the knowledge of DFT derived Wannier function overlaps and the low-energy tight-binding Hamiltonian defined in the Wannier basis, we next explore the interplay between hopping interaction (t), crystal field splitting (Δ), Coulomb interaction (U), Hund's exchange (J_H) and spin-orbit coupling (λ) for the cubic and monoclinic structures by performing many-body multiplet calculations within a two-site problem. This enables us with the opportunity to explore

the parameter space in an accurate manner.

The two-site Os t_{2g} only model Hamiltonian taking into account the effect of hopping, Coulomb interaction, and spin-orbit coupling is given by,[41–43]

$$\begin{aligned}
H &= H_{\text{onsite}} + H_{\text{int}} + H_{\text{SO}} + H_t \\
H_{\text{onsite}} &= \sum_i \sum_{l,m} \Delta_{l,m}^i d_{i,l\sigma}^\dagger d_{i,m\sigma} \\
H_{\text{int}} &= U \sum_i \sum_l n_{i,l\uparrow} n_{i,l\downarrow} + \frac{(U' - J_H)}{2} \sum_i \sum_{\substack{l,m \\ l \neq m}} n_{i,l\sigma} n_{i,m\sigma} \\
&+ \frac{U'}{2} \sum_i \sum_{\substack{l,m \\ l \neq m \\ \sigma \neq \sigma'}} n_{i,l\sigma} n_{i,m\sigma'} - \frac{J_H}{2} \sum_i \sum_{\substack{l,m \\ l \neq m}} (d_{i,m\uparrow}^\dagger d_{i,m\downarrow} d_{i,l\downarrow}^\dagger d_{i,l\uparrow} \\
&+ d_{i,m\uparrow}^\dagger d_{i,m\downarrow}^\dagger d_{i,l\downarrow} d_{i,l\uparrow} + h.c.) \\
H_{\text{SO}} &= \frac{i\lambda}{2} \sum_i \sum_{\substack{l,m,n \\ \sigma,\sigma'}} \epsilon_{lmn} d_{i,l\sigma}^\dagger d_{i,m\sigma'} \sigma_{\sigma,\sigma'}^n \\
H_t &= \sum_{\substack{l,m,\sigma \\ < i,j >}} t_{lm}^{ij} (d_{i,l\sigma}^\dagger d_{j,m\sigma} + h.c.)
\end{aligned}$$

$d_{i,l\sigma} (d_{i,l\sigma}^\dagger)$ is the annihilation (creation) operator of the l^{th} orbital ($l = 1-3 \in t_{2g}$) with a spin σ at site i and $n_{i,l\sigma} = d_{i,l\sigma}^\dagger d_{i,l\sigma}$. λ implies the strength of spin-orbit coupling in H_{SO} . t_{lm}^{ij} is the nearest-neighbor hopping between l^{th} orbital of site i and m^{th} orbital of site j . H_{onsite} represents the on-site energies of the Os t_{2g} orbitals. Pure cubic environment of Os leads to degenerate t_{2g} levels for the cubic structure while all t_{2g} levels are split due to non-cubic distortion in monoclinic phase. H_{int} in the Kanamori representation contains intra-orbital coulomb correlation (U), Hund's coupling strength (J_H), inter-orbital coulomb correlation (U'). The first term of H_{int} costs an energy U to stabilize the state counteracting intra-orbital electron-electron repulsion. Hund's coupling (J_H) in the second term lowers the energy of states having same spin in multiple orbitals. The inter-orbital Coulomb interaction satisfies the relation $U' = U - 2J_H$. The realistic values of non-cubic crystal field and the inter-site hopping parameters are obtained from NMTO[35] downfolding calculations, described above, while U and J_H parameters are varied over physically meaningful range ($U' > J_H$) with λ values fixed at 0.1 eV, 0.2 eV and 0.4 eV. Energy difference between parallel and anti-parallel alignment of Os spins is then studied by exact diagonalization of the above two site problem.[44] The results are summarized in Fig. 3. The energy differences with a choice of $U = 2$ eV and $\lambda = 0.1$ eV upon varying strength of J_H are plotted in Figs 3(a) and 3(b) for cubic and monoclinic structures respectively. This brings out an important observation. While for the cubic phase, the parallel alignment of Os spin or ferromagnetic interaction becomes favoured over antiferromagnetic interaction beyond a

J_H value of 0.27 eV or so, for the monoclinic structure the ferromagnetic interaction gets stabilized over antiferromagnetic interaction only beyond J_H value of 0.6 eV. For a choice of $J_H = 0.6$ eV, a reasonable estimate for 5d TM like Os, one would thus find the FM interaction is stabilized for cubic and AFM interaction is stabilized for monoclinic structure. Further to this, while the ferro interaction is stabilized over antiferro in the cubic phase by a large energy gain of almost about 30 meV, giving rise to a mean field temperature scale, $\frac{zJs^2}{3}$ (z being number of nearest-neighbor which is 12) above 1300 K, the corresponding stabilization of AFM interaction over FM interaction in the monoclinic phase is only about 1.5 meV, translating to a mean field temperature scale of only ~ 70 K. One would thus expect ferromagnetic state to support a large T_c , and antiferromagnetic state to exhibit a low transition temperature – a trend found between the reported cubic structured Sr_3OsO_6 [18] and monoclinic structured Ca_3OsO_6 . [23] A very similar situation is obtained for higher values of $\lambda = 0.2$ eV and 0.4 eV. The resultant $U - J_H$ phase diagram for $\lambda = 0.2$ eV and 0.4 eV are shown in Figs 3(c) and 3(d) respectively. The two phase diagrams appear qualitatively same, except the increase of λ value shifts the transition from antiferro to ferro to slightly larger value of J_H , as spin-orbit coupling tend to favour antiferromagnetism. We find that in both choices of λ values, the ferromagnetic interaction gets stabilized only in a tiny part of the $U - J_H$ phase space in monoclinic structure, while a significant part of $U - J_H$ phase space supports ferromagnetic interaction in cubic structure. Summarizing these observations, one would thus expect that ferromagnetic phase to be comfortably stabilized in cubic structure of Sr_3OsO_6 with a rather high temperature scale, while the monoclinic structure would mostly favour antiferromagnetic interaction with a low transition temperature. The antiferromagnetism being frustrated within the FCC motif of the Os sublattice it may also give rise to spin-glass like behaviour in compound specific cases. Repeating the calculation considering triclinic symmetry of Sr_3OsO_6 , one of the suggested structure of bulk Sr_3OsO_6 in Ref.40 and the next favored theoretically suggested structure, the $U - J_H$ phase diagram for all choices of λ is found to consist of solely antiferromagnetic phase, implying ferromagnetic interaction to be disfavored even more in the triclinic phase, compared to the monoclinic phase. This is in complete agreement with the observation of antiferromagnetism rather than ferromagnetism in bulk Sr_3OsO_6 . [40]

Since the ferromagnetic interaction is favoured by hopping between occupied and empty orbitals the stabilized ferromagnetic phase also shows orbital ordering of two occupied orbitals between the four sites of FCC tetrahedra, as shown schematically in inset of Fig. 3(c). The two sites connected through (1,1,0) vector are found to have the electron occupancy mostly at d_{xz}/d_{yz} and d_{xz}/d_{xy} orbitals, promoting hopping between filled and empty d_{xy} orbitals. Similarly orbital occupancy's at sites connected through (1,0,1) and (0,1,1) vectors favor hopping between filled to empty d_{xz} and d_{yz} orbitals, respectively.

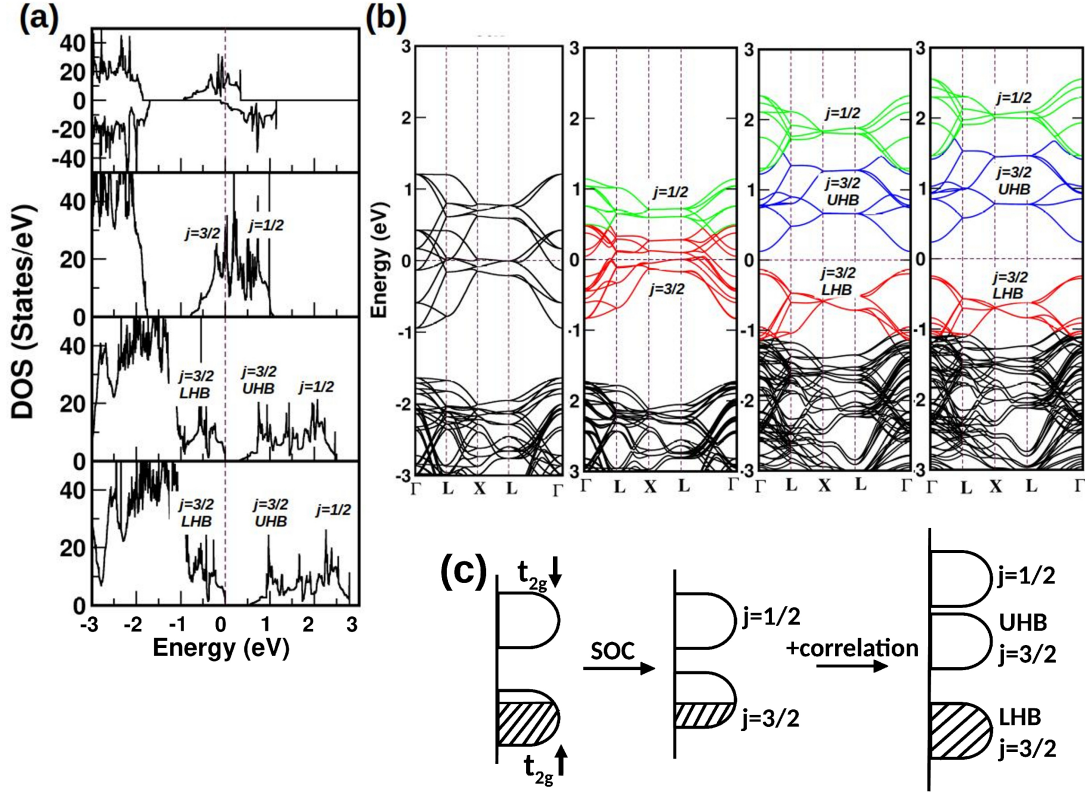


FIG. 4: (Color online) (a) The density states of cubic Sr_3OsO_6 computed within spin-polarized GGA, GGA+SOC, GGA+SOC+U [$U = 2$ eV] and GGA+SOC+U [$U = 3$ eV] (from top to bottom). Marked are the spin-orbit coupled $j = 3/2$ and $j = 1/2$ manifolds, which in presence of correlation effect U develops into $j = 3/2$ LHB and $j = 3/2$ UHB. See text for details. (b) The band structures of cubic Sr_3OsO_6 plotted along high symmetry points of the FCC BZ, within GGA, GGA+SOC, GGA+SOC+U [$U = 2$ eV] and GGA+SOC+U [$U = 3$ eV] (from left to right). For spin-polarized GGA band structure, the bands corresponding to majority spin channel is only shown. The bands corresponding to $j = 3/2$ (LHB, UHB) and $j = 1/2$ are colored differently. The zero of the energy in both density of states and band structure plots is fixed at respective Fermi level. (c) The systematic effect of turning on SOC and U on Os t_{2g} s in d^2 configuration, shown schematically. The filled states are represented as hatched.

Insulating Electronic Structure

Having unraveled the stabilization of ferromagnetic state in cubic Sr_3OsO_6 being driven by the large Os-Os nearest neighbor hopping mediated by bending of O p tails of Os t_{2g} Wannier functions towards the Sr_A atoms at A sites, we next explore the origin of insulating behavior of ferromagnetic, cubic Sr_3OsO_6 . In order to disentangle various influencing factors in driving the insulating state, in steps we carry out calculations within the framework of GGA, GGA+SOC and GGA+SOC+ U .

With two electrons occupying three degenerate t_{2g} levels of Os in an ideal cubic environment, GGA calculation leads to metallic solution (cf top panel of Fig. 4(a)) with a magnetic moment of $1.10 \mu_B$ at Os site, and $0.05 \mu_B$ at O site due to finite Os-O covalency. Inclusion of spin-orbit coupling within GGA+SOC, develops a significant orbital moment of $-0.17 \mu_B$ at Os site, oppositely aligned to spin moment of $0.62 \mu_B$ at Os site, in conformity with less than half-filled nature of Os occupancy. As is seen from the density of states and band structure plots, presented in Fig. 4(a)-(b), inclusion of

SOC, keeps the solution metallic with Os states crossing the Fermi level. The situation is schematically shown in panel (c) of Fig. 4. Switching of spin-orbit coupling mixes the up and down spin channels of t_{2g} 's, which effectively behave as $l=1$ quantum number states. The states in presence of spin-orbit coupling thus are described by four fold degenerate $j = 3/2$ and two fold degenerate $j = 1/2$ states. With d^2 occupancy of Os, the $j = 3/2$ states therefore become half-filled, a situation very similar to d^5 Iridate like Sr_2IrO_4 which results in half-filled $j = 1/2$ states instead of half filled $j = 3/2$ states in the present case.[31] Akin to Sr_2IrO_4 , one would thus expect inclusion of onsite correlation, U , modeled within a GGA+SOC+ U framework would be able to open up gap. This expectation turned out to be true where a gap within $j = 3/2$ manifold is found to open up for a choice of U value ≥ 2 eV. As shown in Fig. 4(b), within the GGA+SOC+ U description, out of 24 t_{2g} bands of Os in a 4 f.u. cubic cell, 8 of the bands lie below the Fermi level, forming $j = 3/2$ lower Hubbard bands (LHB), while rest 16 of the bands lie above Fermi level, separated by a gap from $j = 3/2$ LHB states. Eight empty $j = 3/2$ upper Hubbard bands (UHB)

overlap with eight empty $j = 1/2$ bands due to finite band widths of $j = 3/2$ and $j = 1/2$. With inclusion of Hubbard U correction, both the spin moment and orbital moment of Os show an increase with values $1.48 \mu_B$ and $-0.65 \mu_B$ respectively for choice of $U = 2$ eV. This leads of a magnetic moment of $0.83 \mu_B$, in good agreement with experimentally measured[18] moment of $0.77 \mu_B$. Like a Mott insulator, the gap value is found to scale with U , with calculated band gap value of 0.33 eV for $U = 2$ eV and 0.55 eV for $U = 3$ eV. Thus Sr_3OsO_6 forms an example of spin-orbit entangled Mott state in $j = 3/2$ sector, similar to that of Sr_2IrO_4 in $j = 1/2$ sector.

SUMMARY AND DISCUSSION

In this study, we take up the case of Os containing double perovskite compound, Sr_3OsO_6 , and study the microscopic origin of its reported high T_c ferromagnetic insulating behavior.[18] It is curious to note that while cubic crystal structure of Sr_3OsO_6 has been reported in Ref.18 grown as thin film, a recent report of bulk Sr_3OsO_6 compound synthesized via solid-state route suggests the crystal structure to be in non-cubic monoclinic or triclinic symmetry.[40] We thus start our study by exploring the crystal symmetry of Sr_3OsO_6 predicted via application of genetic algorithm together with first-principles total energy calculations. These calculations show monoclinic symmetry as most preferred symmetry followed by triclinic symmetry, while the cubic symmetry structure lie energetically much higher.

Following this finding, we explore the influence of crystal symmetry on the magnetic properties by considering the predicted lowest energy monoclinic structure and the reported[18] cubic structure. Towards this end, employing first-principles derived Wannier representation of Os t_{2g} orbitals, we first show that Os-Os super-exchange is primarily governed by counter-intuitive large Os-Os hopping across the face of the cubic structure, which dominates over conventionally expected Os-O-Sr_B-O-Os super-exchange path along the edge of the cubic structure. This hopping process, which is caused by Sr-O covalency driven bending of O p like tails of the Os t_{2g} effective Wannier functions, gets substantially reduced in the distorted monoclinic phase due to misalignment of O p like tails. Using DFT derived Os t_{2g} low energy Hamiltonian defined in the Wannier basis, we next solve the two-site Os t_{2g} full multiplet problem within exact diagonalization scheme in t - U - J_H - λ space. We find a crossover from antiferro alignment of Os spins to ferro alignment of Os spins happens in U - J_H space for several choices of λ values. For the choice of λ values relevant for Os, a large part of U - J_H phase diagram in cubic symmetry is found to support ferro alignment of Os spins. On the contrary, ferro phase is found to be largely suppressed in monoclinic symmetry, the phase space being primarily dominated by antiferro alignment of Os spins. Interestingly, for choice of same parameter values of U , J_H and λ , the stabilization energy of ferro alignment over antiferro in the cubic phase is found to be more than order

of magnitude larger compared to stabilization energy of anti-ferro alignment of Os spins over ferro in distorted monoclinic phase. This rationalizes the observation of high T_c in reported cubic, FM phase of Sr_3OsO_6 and low Neél temperature in reported monoclinic, AFM phase of Ca_3OsO_6 . This analysis establishes that the stabilization of cubic phase of Sr_3OsO_6 in Ref.18, was crucial to its observed high T_c ferromagnetism. Following this understanding, we investigate the origin of insulating behavior of FM Sr_3OsO_6 through systematic analysis of GGA, GGA+SOC and GGA+SOC+ U scheme of electronic structure calculations. While both GGA and GGA+SOC calculations lead to metallic solutions, insulating ground state is achieved only within the treatment of GGA+SOC+ U with reasonable choices of U values. This characterizes the insulating state in cubic Sr_3OsO_6 as $j = 3/2$ Mott state induced by large spin-orbit coupling at Os site.

Finally, searching for related double perovskite candidates, exhibiting high T_c FM insulating state, $\text{Sr}_2\text{CaOsO}_6$ appear to be a promising candidate. With Sr at A site, and Ca at B' site, the tolerance factor of this compound turns out to be 0.93. Following the expectation from the tolerance factor, the powder X-ray diffraction analysis[15] of synthesized $\text{Sr}_2\text{CaOsO}_6$ suggested an ordered cubic structure. Calculated Os-Os hopping strengths in NMTO-downfolding scheme of Wannier representation in $\text{Sr}_2\text{CaOsO}_6$ turn out to be rather similar to that of cubic Sr_3OsO_6 , the largest Os-Os hopping being 0.16 eV compared to 0.17 eV in Sr_3OsO_6 . While there exists report of synthesis of this compound,[15] to the best of our knowledge its magnetic property, so far remains unexplored. This raises the hope that the bulk form of $\text{Sr}_2\text{CaOsO}_6$ should also support high T_c ferromagnetism. In view of our study, it will be worth while to take this up.

ACKNOWLEDGEMENT

T.S-D acknowledges computational support under Thematic Unit of Excellence funded by Department of Science and Technology, India. T.S-D thanks Arun Paramakanti or useful discussions. I.D thanks Science and Engineering Research Board (SERB), India (Project No. EMR/2016/005925) for financial support.

* Electronic address: t.sahadasgupta@gmail.com

- [1] D.D. Sarma, Current Opinion in Solid State and Materials Science, **5**, 261 (2001).
- [2] S. Vasala and M. Karppinen, Prog. Solid State Chem. **43**, 1 (2015).
- [3] T. Saha-Dasgupta, J. Supercond. Nov. Magn. **26**, 1991 (2013).
- [4] Hai L. Feng, Madhav Prasad Ghimire, Zhiwei Hu, Sheng-Chieh Liao, Stefano Agrestini, Jie Chen, Yahua Yuan, Yoshitaka Matsushita, Yoshihiro Tsujimoto, Yoshio Katsuya, Masahiko Tanaka, Hong-Ji Lin, Chien-Te Chen, Shih-Chang Weng, Manuel Valvidares, Kai Chen, Francois Baudelet, Arata

- Tanaka, Martha Greenblatt, Liu Hao Tjeng, and Kazunari Yamaura Phys. Rev. Materials **3**, 124404 (2019).
- [5] Hai L. Feng, Stuart Calder, Madhav Prasad Ghimire, Ya-Hua Yuan, Yuichi Shirako, Yoshihiro Tsujimoto, Yoshitaka Matsushita, Zhiwei Hu, Chang-Yang Kuo, Liu Hao Tjeng, Tun-Wen Pi, Yun-Liang Soo, Jianfeng He, Masahiko Tanaka, Yoshio Katsuya, Manuel Richter, and Kazunari Yamaura Phys. Rev. B **94**, 235158 (2016).
- [6] Y. Tomioka, T. Okuda, Y. Okimoto, R. Kumai, K.-I. Kobayashi, Y. Tokura, Phys. Rev. B **61**, 422 (2000).
- [7] P. Sanyal, H. Das, and T. Saha-Dasgupta, Phys. Rev. B **80**, 224412 (2009).
- [8] T. K. Mandal, C. Felser, M. Greenblatt, and Jurgen Kubler, Phys. Rev. B **78**, 134431 (2008).
- [9] P. Sanyal, A. Halder, L. Si, M. Wallerberger, K. Held, and T. Saha-Dasgupta, Phys. Rev. B **94**, 035132 (2016).
- [10] J. B. Phillip, P. Majewski, L. Alff, A. Erb, R. Gross, T. Graf, M. S. Brandt, J. Simon, T. Walther, W. Mader, D. Topwal, and D. D. Sarma, Phys. Rev. B **68**, 144431 (2003).
- [11] H. Das, P. Sanyal, T. Saha-Dasgupta, and D. D. Sarma, Phys. Rev. B **83**, 104418 (2011).
- [12] M. De Teresa, D. Serrate, C. Ritter, J. Blasco, M. R. Ibarra, L. Morellon, and W. Tokarz, Phys. Rev. B **71**, 092408 (2005).
- [13] C. M. Thompson, J. P. Carlo, R. Flacau, T. Aharen, I. A. Leahy, J. R. Pollichiemi, T. J. S. Munsie, T. Medina, G. M. Luke, J. Munevar, S. Cheung, T. Goko, Y. J. Uemura, and J. E. Greedan, Journal of Physics: Condensed Matter **26**, 306003 (2014).
- [14] Y. Yuan, H. L. Feng, M. P. Ghimire, Y. Matsushita, Y. Tsujimoto, J. He, M. Tanaka, Y. Katsuya, and K. Yamaura, Inorganic Chemistry **54**, 3422 (2015).
- [15] R. Morrow, A. E. Taylor, D. J. Singh, J. Xiong, S. Rodan, A. U. B. Wolter, S. Wurmehl, B. Bchner, M. B. Stone, A. I. Kolesnikov, A. A. Aczel, A. D. Christianson, and P. M. Woodward, Scientific Reports **6**, 32462 (2016).
- [16] A. A. Aczel, Z. Zhao, S. Calder, D. T. Adroja, P. J. Baker, and J.-Q. Yan, Phys. Rev. B **93**, 214407 (2016).
- [17] T. Saitoh, M. Nakajima, A. Kakizaki, H. Nakajima, O. Morimoto, Sh. Xu, Y. Moritomo, N. Hamada, Y. Aiura, Phys. Rev. B **66**, 035112 (2002).
- [18] Y. K. Wakabayashi, Y. Krockenberger, N. Tsujimoto, T. Boykin, S. Tsuneyuki, Y. Taniyasu, H. Yamamoto, Nat Commun. **10** 535, (2019).
- [19] B. T. Matthias, R. M. Bozorth, and J. H. Van Vleck, Phys. Rev. Lett. **7**, 160 (1961).
- [20] P. K. Baltzer, H. W. Lehmann, and M. Robbins, Phys. Rev. Lett. **15**, 493 (1965).
- [21] M. A. Subramanian, A. P. Ramirez, and W. J. Marshall, Phys. Rev. Lett. **82**, 1558 (1999).
- [22] H. Das, U. V. Waghmare, T. Saha-Dasgupta, and D. D. Sarma, Phys. Rev. Lett. **100**, 186402 (2008).
- [23] H. L. Feng, Y. Shi, Y. Guo, J. Li, A. Sato, Y. Sun, X. Wang, S. Yu, C. I. Sathish and K. Yamaura, Journal of Solid State Chemistry **201**, 186, (2013).
- [24] J. H. Choy, D. K. Kim, J. Y. Kim, Solid State Ionics **108**, 159 (1998).
- [25] V. Heine, "The Pseudopotential Concept", Solid State Physics, Solid State Physics, Academic Press, **24**, pp. 1-36, (1970), doi:10.1016/S0081-1947(08)60069-7, ISBN 9780126077247.
- [26] O. K. Andersen, Phys. Rev. B **12**, 3060 (1975).
- [27] G. Kresse and J. Hafner, Phys. Rev. B **47**, R558 (1993), G. Kresse and J. Furthmüller, Phys. Rev. B **54**, 11169 (1996).
- [28] John P. Perdew, J. A. Chevary, S. H. Vosko, Koblar A. Jackson, Mark R. Pederson, D. J. Singh, and Carlos Fiolhais, Phys. Rev. B **48**, 4978(E) (1993).
- [29] J. P. Perdew, K. Burke, and M. Ernzerhof, Phys. Rev. Lett. **77**, 3865 (1996).
- [30] A. I. Liechtenstein, V. I. Anisimov and J. Zaanen, Phys. Rev. B **52**, R5467 (1995).
- [31] B. J. Kim, Hosub Jin, S. J. Moon, J.-Y. Kim, B.-G. Park, C. S. Leem, Jaeyun Yu, T. W. Noh, C. Kim, S.-J. Oh, J.-H. Park, V. Durairaj, G. Cao, and E. Rotenberg, Phys. Rev. Lett. **101**, 076402 (2008).
- [32] Guoqiang Lana, Jun Song, Zhi Yang, J. Alloy. Comp. **749** 909 (2018).
- [33] A. Neroni, E. Sasloglu, H. Hadipour, C. Friedrich, S. Blügel, I. Mertig, and M. Lezaic, Phys. Rev. B **100**, 115113 (2019).
- [34] Ersoy Sasoglu, Christoph Friedrich, and Stefan Blügel, Phys. Rev. B **83**, 121101(R) (2011).
- [35] O. K. Andersen and T. Saha-Dasgupta, Phys. Rev. B **62**, R16219 (2000).
- [36] O.K. Andersen and O. Jepsen, Phys. Rev. Lett. **53**, 2571 (1984).
- [37] Oganov, A. R. & Glass, C.W. Crystal structure prediction using ab initio evolutionary techniques: Principles and applications. *J. Chem. Phys.* **124**, 244704-244718 (2006); Lyakhov, A.O., Oganov, A.R. & Valle, M. In *Modern Methods of Crystal Structure Prediction*; Oganov, A.R., Eds.; Wiley-VCH Verlag GmbH & KGaA : Weinheim, Germany, 2012; Chapter Crystal structure prediction using evolutionary approach, pp 147-180.; Oganov A.R. & Glass C.W. Evolutionary crystal structure prediction as a tool in materials design. *J Phys: Condens Matter* **20**, 064210-064215 (2008).
- [38] A. Halder, D. Nafday, P. Sanyal, T. Saha-Dasgupta, npj Quantum Materials **3**, 17 (2018)
- [39] Anita Halder, Aishwaryo Ghosh, and Tanusri Saha Dasgupta Phys. Rev. Materials **3**, 084418 (2019).
- [40] J. Chen et al., arXiv2002.06743
- [41] H. Matsuura and K. Miyake, J. Phys. Soc. Jpn. **82**, 073703 (2013).
- [42] A. Chakraborty and I. Dasgupta, Journal of Magnetism and Magnetic Materials **492**, 165708 (2019).
- [43] A. Nag, S. Bhowal, A. Chakraborty, M. M. Sala, A. Efimenko, F. Bert, P. K. Biswas, A. D. Hillier, M. Itoh, S. D. Kaushik, V. Siruguri, C. Meneghini, I. Dasgupta, and S. Ray, Phys. Rev. B **98**, 014431 (2018).
- [44] H. Meskine, H. Konig, and S. Satpathy, Phys. Rev. B **62**, 094433 (2001).